ELSEVIER

Contents lists available at ScienceDirect

# Science of the Total Environment

journal homepage: www.elsevier.com/locate/scitotenv



# Identifying sources and cycling of phosphorus in the sediment of a shallow freshwater lake in China using phosphate oxygen isotopes



Hezhong Yuan <sup>a,b</sup>, Qiang Li <sup>b</sup>, Ravi K. Kukkadapu <sup>c</sup>, Enfeng Liu <sup>d</sup>, Jianghua Yu <sup>a</sup>, Hao Fang <sup>a</sup>, Hui Li <sup>b</sup>, Deb P. Jaisi <sup>b,\*</sup>

<sup>a</sup> School of Environmental Science and Engineering, Nanjing University of Information Science & Technology, Nanjing, Jiangsu 210044, PR China

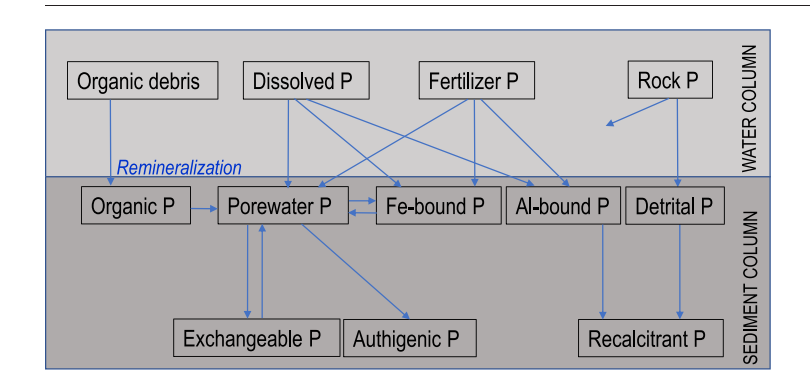
ABSTRACT

- <sup>b</sup> Department of Plant and Soil Sciences, University of Delaware, Newark, DE 19716, United States
- <sup>c</sup> Environmental Molecular Sciences Laboratory, Pacific Northwest National Laboratory, Richland, WA 99354, United States
- <sup>d</sup> College of Geography and Environment, Shandong Normal University, Ji'nan, Shandong 250359, PR China

#### HIGHLIGHTS

- Sediment P pools provide information on the size of labile P and recalcitrant P sinks.
- δ<sup>18</sup>O<sub>P</sub> values can differentiate sources and pathways of formation of P pools.
- Isotopes of Al bound P is a better recorder of terrestrial P sources than Febound P pool.

#### GRAPHICAL ABSTRACT



# ARTICLE INFO

Article history: Received 17 February 2019 Received in revised form 12 April 2019 Accepted 21 April 2019 Available online 23 April 2019

Keywords:
Sources and cycling
Phosphorus
Sediment
<sup>57</sup>Fe-Mössbauer spectroscopy
Phosphate oxygen isotopes

ry 2019 shallow fr

Biotic and abiotic pathways for the transformation of phosphorus (P) in the sediment of Taihu Lake, a eutrophic shallow freshwater lake in southeastern China, were studied using the oxygen isotope ratios of phosphate ( $\delta^{18}O_P$ ) along with sediment chemistry, X-ray diffraction, and  $^{57}\text{Fe-M\"ossbauer}$  spectroscopic methods. The results showed that  $\delta^{18}O_P$  values of sediment P pools significantly deviated from equilibrium and thus allowed distinguishing potential P sources or pathways of transformation. Isotope values of authigenic P being lighter than equilibrium suggests the re-mineralization of organic matter and subsequent precipitation of apatite as the major pathway of formation of authigenic P. The  $\delta^{18}O_P$  values of the Al-bound P pool (18.9–23.5%) and ferric Fe-bound P (16.79–19.86%) could indicate potential terrestrial sources, but the latter being closer to equilibrium values implies partial overprinting of potential source signature, most likely due to reductive dissolution and release of P and followed by partial biological cycling before re-sorption/re-precipitation with newly formed ferric Fe minerals. Oxic/anoxic oscillation and dissolution/re-precipitation reactions and expected isotope excursion are corroborated by sediment chemistry and Mössbauer spectroscopic results. These findings provide improved insights for better understanding the origin and biogeochemical cycling of P associated with eutrophication in shallow freshwater lakes.

© 2019 Elsevier B.V. All rights reserved.

\* Corresponding author. E-mail address: jaisi@udel.edu (D.P. Jaisi).

# 1. Introduction

Phosphorus (P) is an essential nutrient and component of major structures for all living beings and thus is required for all life and for healthy aquatic ecosystems (Karl, 2000). In freshwater bodies, excess P input from point and/or non-point external sources, as well as that recycled within the water body, accelerates eutrophication (Gächter and Wehrli, 1998; Fink et al., 2018). Shallow lakes are usually well mixed and often oxic throughout the water column due to physical factors such as waves (Deng et al., 2018). However, the shallow sediment of such lakes can be anoxic and release P to overlying oxic lake water due to redox changes (Linge et al., 2004). Characterizing P pools, forms and cycling in shallow freshwater lakes affected by non-point nutrient sources is a priority task for identifying the relative contribution of anthropogenic P loading which in turn provides useful information for formulating effective nutrient management strategies.

Natural and anthropogenic sources of P are more common in many lake and coastal environments (Linge et al., 2004; Reed et al., 2011). Solid phase P transferred from terrestrial sources to aquatic ecosystems could be partially preserved in sediment P reservoirs including Fe-(oxy) hydroxides or dissolved to form authigenic minerals (Ruttenberg, 1992). Phosphorus bound to minerals in the sediment is conditionally bioavailable for organisms in aquatic environments, depending on the chemical form of P such as sorbed, co-precipitated, physically occluded, or imposed ambient conditions (Jaisi et al., 2011). Biotic and abiotic reactions can occur concurrently to dissolve or precipitate P and redistribute P from one pool/phase to another (Markel et al., 1994). Identification and tracking of sources and biological availability of different P pools based on operationally defined sequential extraction procedures are not straightforward because of the diversity of the autochthonous and allochthonous sources and variable rate of recycling of different P pools in the sediment.

Since the pioneering work initiated by Longinelli and Nuti (1973), phosphate oxygen isotope ratios ( $\delta^{18}O_P$ ) have been used primarily as paleo-environmental proxies (Pucéat et al., 2010; Jaisi and Blake, 2010) and more recently as a tracer of sources and cycling of P as well as to infer microbial activities in the modern aquatic environment (Blake et al., 2005; Colman et al., 2005; Elsbury et al., 2009). The covalent P-O bond in phosphate is fairly resistant to isotope exchange with water at low temperature, near-neutral pH, and earth-surface pressures for a long time (Lecuyer et al., 1999). The isotope exchange is only possible in enzyme-mediated reactions which imprint equilibrium isotope compositions (Blake et al., 2001). Hydrolysis of organic P generates disequilibrium fractionation effects which depend on the composition of enzyme and substrate (Liang and Blake, 2006, 2009; von Sperber et al., 2014). Thus, any measured variability in isotopic composition could reflect the abiotic mixing of isotopically distinct P sources, variably exchanged with water, or hydrolyzed from different organic P compounds. Analysis of  $\delta^{18}O_p$  may offer new insights into the source identification of phosphorus in aquatic ecosystems including marine, estuarine, freshwater, and sediment (Davies et al., 2014).

Diagenetic processes may cause dissolution of minerals and release of P bound to them, which may re-sorb to other or new mineral surfaces (Jaisi and Blake, 2010). Therefore,  $\delta^{18} O_P$  values of different P pools possibly overprint or change toward equilibrium isotope composition in the sediment column. Most recently, Joshi et al. (2015) found that organic matter remineralization was the predominant pathway of P

cycling in the sediment of the Chesapeake Bay, USA, and the role of Fe-bound P in the sediment to release inorganic phosphorus  $(P_i)$  was found negligible. Similarly, at the Peru Margin,  $\delta^{18}O_P$  values suggested that sources of authigenic P were driven from enzyme-catalyzed hydrolysis of organic matter (Jaisi and Blake, 2010). Laboratory incubation studies are used to confirm that the isotopic compositions of Fe-oxide bound P largely retain their original isotope signatures during dissolution and precipitation (Jaisi et al., 2011), and P pools such as authigenic and detrital, unless utilized by bacteria, do not change their isotope composition. In this research, a systematic study on sedimentary P pools of Taihu Lake, a shallow freshwater lake in east China, was performed using a modified SEDEX sequential extraction method and the  $\delta^{18}O_P$  values of each P pool were measured. Sources and potential transformation of P pools are discussed with emphasis on the likely role in the P budget in the water column.

#### 2. Materials and methods

# 2.1. Samples collection and preprocessing

The overlying water samples were collected into a CTD rosette-type custom built water sampler and sediment cores were taken using a columnar sampler in June 2017 from eutrophic Zhushan Bay (N31.42028°, E120.04461°) located in the northwest region of the Taihu Lake, China (Fig. S1). The upper 20 cm of sediment cores were sliced into 1 cm intervals in the field and put into sealable polyethylene bags sterilized with ethylene oxide and stored in a cooler before transported into the laboratory. The sub-samples were lyophilized using a freeze dryer and ground and then separated through a 100 mesh sieve in preparation for subsequent laboratory analyses. The pore water samples were extracted by centrifugation and collected in 10 mL vials for chemical properties and isotope analyses. The surface water samples collected from this site were also analyzed.

Temperature (T), pH, and oxidation-reduction potential (Eh) of each water sample and sediment slice were promptly measured in situ with an in-situ IQ probe (IQmeter IQ-150, USA). Chl a concentration in the water was detected using a multiparameter water quality analyzer (YSI 6600, USA). Inorganic P (P<sub>i</sub>) concentration in the water samples were determined with the phosphomolybdate blue method after passing the solutions through 0.45 µm glass microfiber filters (Whatman GF/ C). Total P and concentrations of other elements including Fe, Mn, Ca, Mg, Al, and S in all water samples were measured by an inductively coupled plasma-optical emission spectrometer (ICP-OES) (Thermo iCAP 7000, USA) after filtering through 0.45 µm glass microfiber filters. Sediment samples were first digested completely for 10 min at 1000 °C in a Katanax K1 Fluxer (Katanax, Canada) and total P and concentrations of other metals were determined using ICP-OES (as above). The concentrations of total organic carbon (TOC) in the sediment were measured by using an elemental analyzer (Leeman CHNO-S, USA) after reacting them with 5% HCl to remove inorganic carbon (IC).

# 2.2. Sequential extraction of P pools

Different P pools in the sediments were extracted by using the SEDEX sequential extraction method originally developed by Ruttenberg (1992) with a minor modification. The sequential extraction was conducted using 8 g sediment at a constant solid/solution ratio of

**Table 1**Properties of surface water of Taihu Lake above the sediment sampling site.

Depth	DO	T	pН	Chl a	PO <sub>4</sub> <sup>3-</sup>	P	Al	Ca	Fe	Mn	$\delta^{18} O_w$	Εδ <sup>18</sup> O <sub>p</sub>	$\delta^{18}O_p^{a}$
m	mg/l	°C		μg/l	mg/l			·			%	·	
2.6	6.4	18.2	8.8	13.4	0.06	0.24	4.2	70.2	0.6	5.5	-6.80	15.51	$14.74 \pm 0.22$

a, n = 3

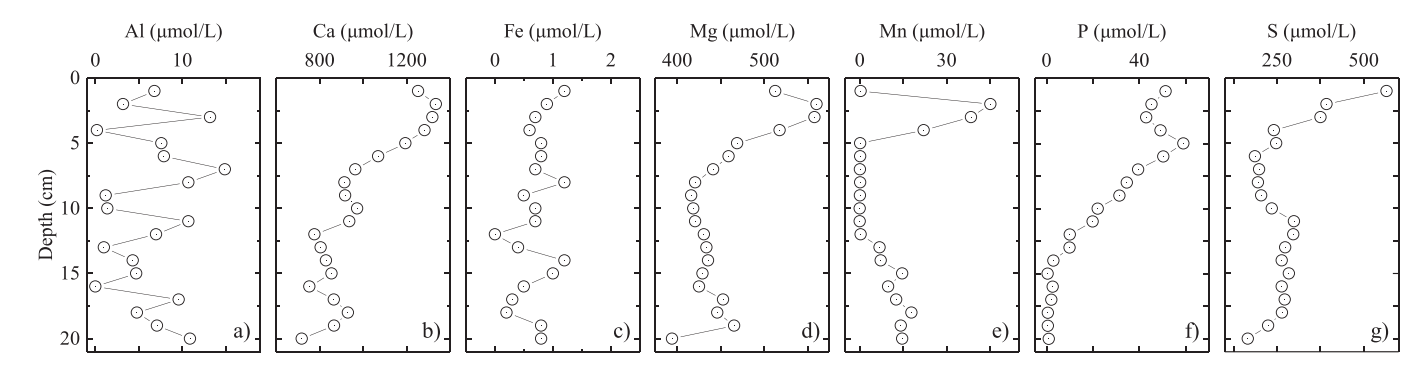


**Fig. 1.** Concentrations of soluble elements (in µmol/L) in the sediment pore water.

1:100 (W:V). The original SEDEX procedure comprises of five steps to differentiate sedimentary P into five major pools: i) exchangeable or loosely sorbed P (exchangeable P), ii) ferric Fe-bound P (Fe-bound P), iii) authigenic carbonate fluorapatite + biogenic apatite + CaCO3-associated P (authigenic P), iv) detrital apatite P of igneous or metamorphic origin (detrital P), and v) residual/recalcitrant organic P (residual  $P_{\rm o}$ ). In this research, the extraction scheme was modified to separate aluminum-oxide bound P (Al-bound P) by inserting a 1.0 M NaOH extraction and NaCO3 wash step after the extraction of the Fe-bound P pool.

#### 2.3. Measurement of phosphate oxygen isotopes

All extracted P pools and lake water samples were further purified to remove contaminants including organic P and concentrated before forming silver phosphate (Ag<sub>3</sub>PO<sub>4</sub>) precipitate for isotope analyses

following the Joshi et al. (2018) method. Silver phosphate was pyrolyzed at 1460 °C using online high-temperature thermal decomposition instrument with thermochemolysis/elemental analyzer (TC/EA) connected to a Delta V continuous flow isotope ratio mass spectrometer (IRMS) (Thermo, Germany). The oxygen yield after pyrolysis was calculated and data with a yield >90% was considered acceptable and included in the analysis. The presence of contaminants was tested by measuring total carbon (TC) and nitrogen (TN) content using a CHN Analyzer connected to the IRMS (Jaisi and Blake, 2014). A few data with unexpected C and/or N content were discarded. The measured  $\delta^{18}\mathrm{O}_{\mathrm{P}}$  values were calibrated against YR series standards and the analytical precision was  $\pm 0.3\%$ .

To determine the water oxygen isotope values ( $\delta^{18}O_w$ ) in surface and pore waters, 0.3 mL of water sample was injected into 12-mL pressurized borosilicate vials prefilled with CO<sub>2</sub> in helium and allowed to equilibrate with H<sub>2</sub>O at 26.2 °C for 24 h. The  $\delta^{18}O_w$  values in H<sub>2</sub>O were

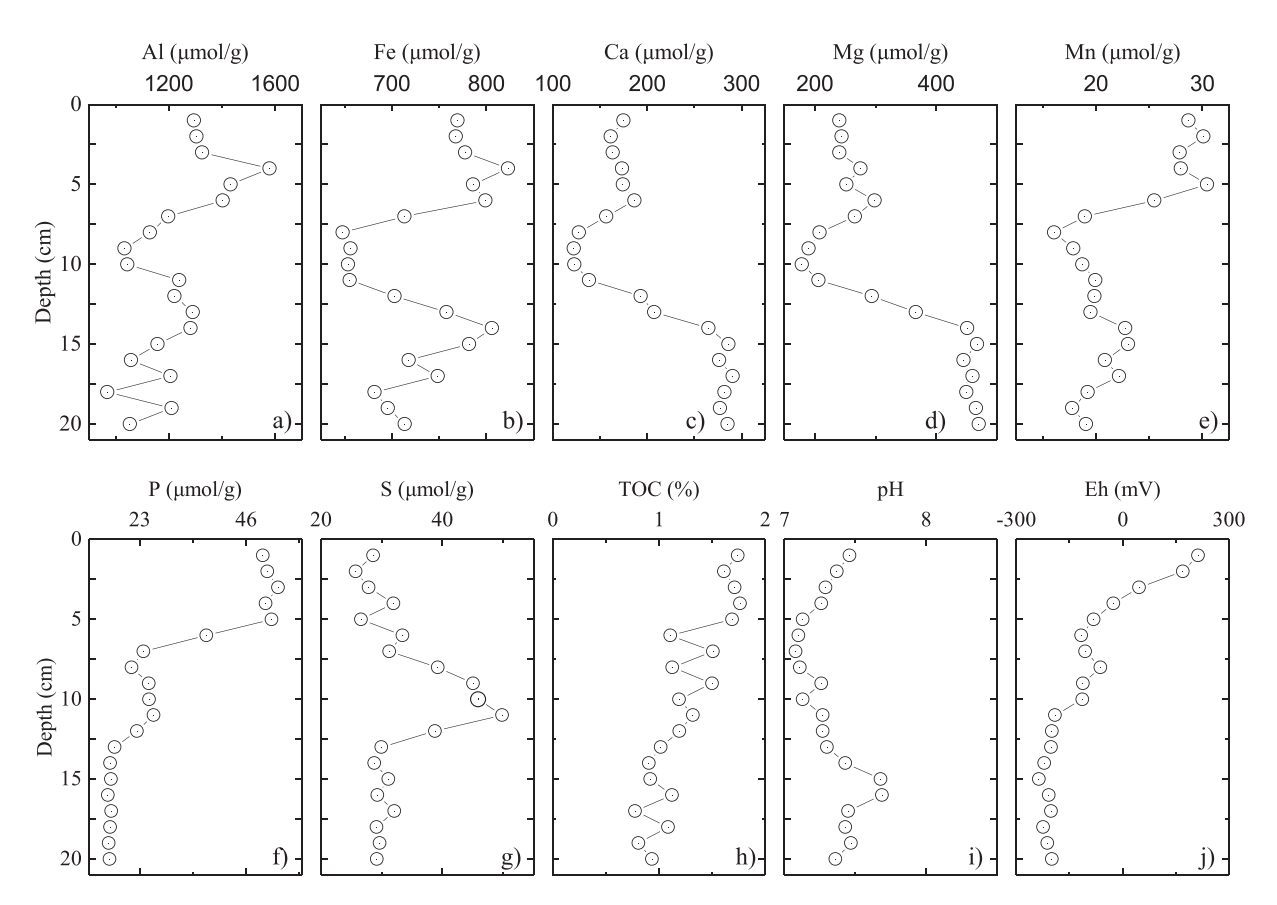


Fig. 2. Elemental concentrations of Al (a), Fe (b), Ca (c) Mg (d), Mn (e), P (f) and S (g), and other physicochemical characteristics (h-j) in the sediment column.

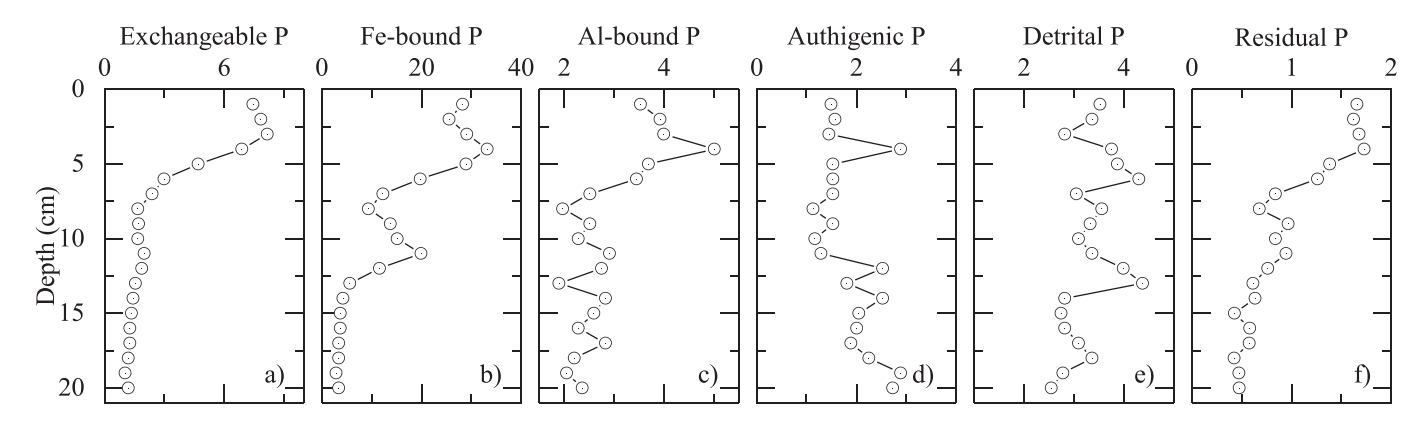


Fig. 3. Depth profiles of different P pool concentrations in the sediment based on revised SEDEX extraction method. Concentrations of P pools are expressed in µmol/g.

then calculated from the measured isotope ratios in CO $_2$  ( $\delta^{18}{\rm O}_{\rm CO2}$ ) based on the known fractionation factor (Cohn and Urey, 1938). The isotope values were measured using a GasBench II coupled with IRMS and calibrated using two USGS standards (W67400 and W32615 with  $\delta^{18}{\rm O}$  of -1.97% and -9.25%, respectively). Triplicate standards were analyzed with a precision >0.06%.

The equilibrium phosphate oxygen isotope composition was calculated following the empirical fractionation equation developed by Chang and Blake (2015):

$$\delta^{18} O_{p} = \left(\delta^{18} O_{W} + 10^{3}\right) \cdot e^{\frac{\left[\left(14.43 \cdot \frac{10^{3}}{1}\right) - 26.54\right]}{10^{3}}} - 10^{3} \tag{1}$$

where  $\delta^{18}O_P$  and  $\delta^{18}O_W$  values refer to the oxygen isotope ratios of phosphate and ambient water in ‰, respectively, and T denotes the measured water temperature in Kelvin (K). All values of  $\delta^{18}O_P$  and  $\delta^{18}O_W$  in this communication are reported with respect to Vienna Standard Mean Ocean Water (VSMOW) at 0‰.

# 2.4. X-ray diffraction (XRD)

Mineralogical analysis was performed from XRD patterns collected from freeze-dried bulk sediment. The sediment was first ground in an agate mortar and sieved through a 100-mesh sieve. XRD analysis of the sediment was performed using Co-K $\alpha$  radiation (40 kV, 40 mA)

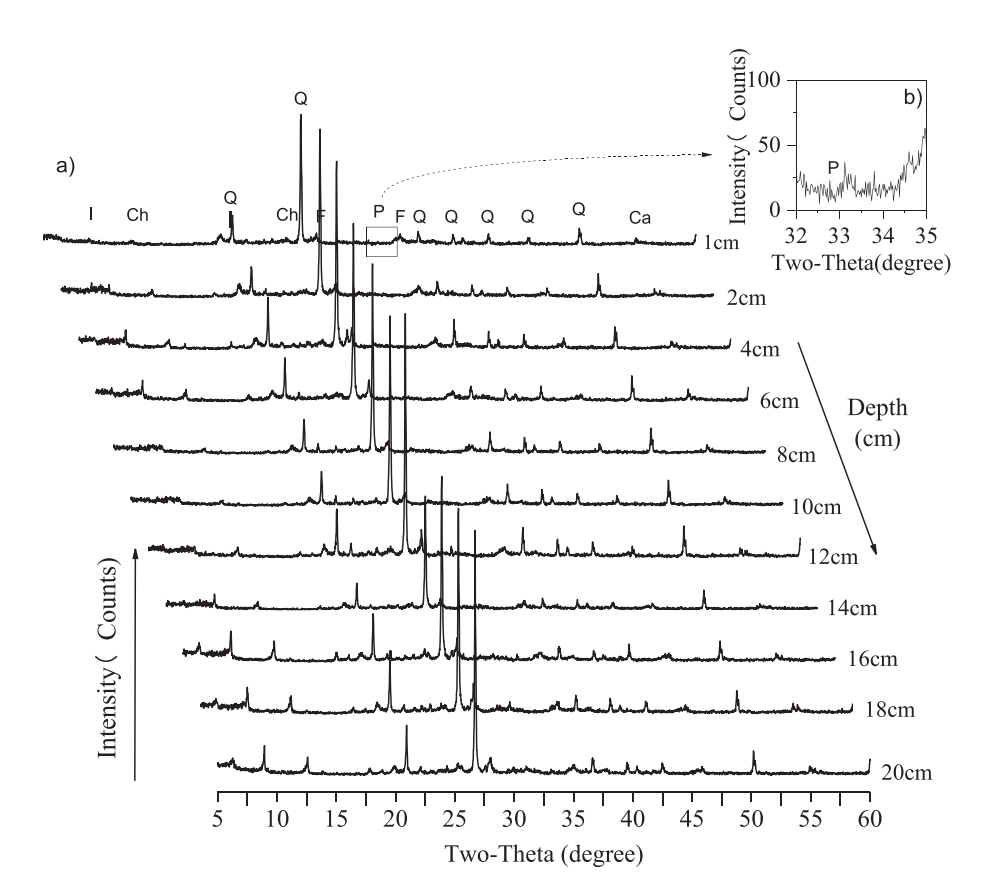


**Fig. 4.** XRD diffraction patterns and mineral phases identified for sediment at different depths. The patterns are background-subtracted (a). Inset (b) shows a high-resolution pattern of local spectra of the selected layer. Ch: chlorite, I: illite, P: pyrite, Q: quartz, F: feldspar, and Ca: calcite. Diffraction peak data refers to the crystalline interplanar spacing (*d*-spacing) and expressed in Å.

on a powder X-ray diffractometer (Bruker D8, Germany) between 5 and 60° 2 $\theta$  angle with a step size of 0.05° 2 $\theta$ /min and a measurement time of 0.02 s per step.

To further identify the clay composition and semi-quantitative analyses of minerals,  $100\,g$  bulk sediment was first washed with  $1000\,m$ L ultrapure water and dispersed in an ultrasonic bath for  $30\,m$ in. It was allowed to settle for  $8\,h$  at  $20\,^{\circ}$ C followed by centrifuging at  $4000\,r$ /s to separate clay fraction. The clay pellets were used to prepare oriented films for XRD analyses. A fraction of pellets was treated with glycol and saturated at  $70\,^{\circ}$ C in an oven for  $1\,h$ . Another fraction was heated at  $550\,^{\circ}$ C in a muffle furnace for  $2\,h$ . Additionally,  $80\,m$ g pelleted clay was treated with  $10\,m$ L of  $5\,M$  HCl and heated in a water bath for  $2\,h$  at  $60\,^{\circ}$ C. After cooling, the mixture was repeatedly washed with ultrapure water until Cl $^-$  was moved completely, and then dried at room temperature (RT). XRD analyses for all three treatments were performed on a Rigaku X-ray diffractometer ( $37.5\,k$ V,  $30\,m$ A) (D/MAX-IIIa, Japan) using Cu K $\alpha$  radiation combing with a graphite monochromator, over a  $3\,a$  and  $35\,^{\circ}$   $20\,$ range with a continuous scanning of  $0.02\,^{\circ}$ /s.

# 2.5. <sup>57</sup>Fe-Mössbauer spectroscopy

Mössbauer spectra of as-received sediment were collected at RT and 13 K using a liquid helium bath cryostat on a conventional constant acceleration spectrometer utilizing a 50 mCi  $^{57}\text{Co/Rh}$  source with the spectrometer in a constant acceleration mode (Wissel MS-500, Germany). This was calibrated with room temperature natural abundance 25  $\mu m$   $\alpha$ -Fe foil. Spectra were fitted using Lorentian line shape function using the least square method. Transmitted radiation was detected using an Ar-Kr proportional counter and the signal was recorded using a 512-channel analyzer. Relative concentrations of the Fe(II) and Fe(III) species were estimated from computed peak areas assuming recoil-free fractions were equal for all the doublets and sextets.

# 3. Results

# 3.1. Chemistry of surface water and pore water

The key chemical properties of surface water are presented in Table 1. High primary productivity is reflected by high Chl a concentration, suggesting eutrophic conditions in the Zhushan Bay. Shallow water depth suggests that dissolved oxygen (DO) can diffuse downwards into the profundal zone due to seasonal change and water turbulence caused by winds. Fig. 1 shows the concentration of  $P_i$  and other elements in pore water at selected sediment depths. The concentrations of  $P_i$  range from 0.6 to 59.0  $\mu$ mol/L and generally decreased with depth. The mean  $\delta^{18}O_P$  value of dissolved P in the water (14.74  $\pm$  0.22%) is close to the calculated average equilibrium value (E $\delta^{18}O_P=15.51\%$ ) indicating rapid enzyme-mediated oxygen exchange and equilibration with ambient water.

High variability of metals and sulfur is observed with depth. Among measured elements (Al, Ca, Fe, Mg, and Mn), Fe concentration is generally lower than others apart from Al. Decreasing Eh values (Fig. 2j) with depth suggest limited penetration and consumption of  $O_2$  in the sediment profile.

# 3.2. Sedimentary P pools

The concentrations of different elements including total P and different P pools in the sediment column along with other ancillary parameters are shown in Figs. 2 and 3. Total P concentrations varied between 16.1 and 53.0 µmol/g. Generally, total P, exchangeable P, Febound P, and Al-bound P concentrations steadily decreased with depth. Most obviously, Fe-bound P, which varied from 2.9 to 33.2 µmol/g, constituted the largest P pool (23.9–65.6% of total P). Exchangeable P comprised the second largest fractions (10.6–17.9%)

on the top 5 cm layer, then sharply reduced to <10%. The Al-bound P and detrital P contributed to increasing fractions of 7.7-21.7% and 6.0-26.2% with depth, respectively. Authigenic P showed a steady increase with depth and widely varied at the range of 3.2-23.9% of total P. The residual  $P_o$  comprised the smallest fraction of the sedimentary P pool (<5%).

#### 3.3. XRD results

Common minerals in the sediment, identified using XRD, were composed predominantly of quartz, chlorite, illite, feldspar, and calcite (Fig. 4). There was no conspicuous difference in mineral compositions with the depth of the sediment that covered approximate 60 years of sedimentation history (calculated from Yuan et al., 2014). Further investigation of bulk sediment verified the occurrence of chlorite and pyrite in association with Fe-containing minerals (Fig. 5). The *d* spacing of untreated samples at 14–15 Å changed to around 17 Å after treatment with glycol, suggesting the presence of montmorillonite. The presence of kaolin was proven by its characteristic peak at 7 Å after treating with HCl. Chlorite has a

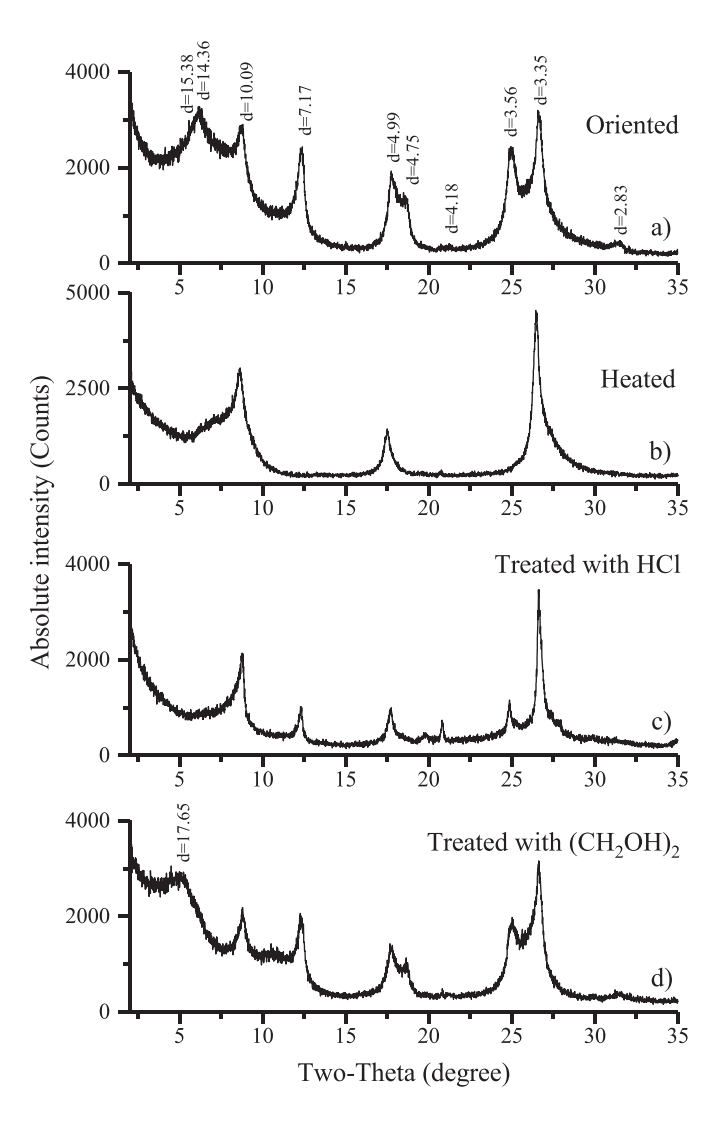


**Fig. 5.** Directional oriented XRD diffraction patterns for bulk sediment under different conditions: a) untreated, b) heated, c) treated with 5 M HCl, and d) treated with glycol ( $CH_2OH_2$ ) to saturation. Note the formation or disappearance of some peaks or shifting to different  $2\Theta$  positions after treatments.

similar peak to kaolin at 7 Å that disappeared after reacting with HCl. Additionally, the peak at 7 Å lost after heating at 550 °C proves the presence of kaolin, and the unaltered peak at 14 Å confirms the presence of chlorite in the sediment.

# 3.4. <sup>57</sup>Fe-Mössbauer spectroscopy

Variable temperature Mössbauer spectroscopy [RT and 13 K; Fig. 6a-1 and a-2] and data summarized in Table 2 provided insights into Fe mineralogy of the sediments. Mössbauer spectral features of 1 cm sediment are consistent with the presence of ferrihydrite-like and phyllosilicate Fe(II)/Fe(III) (chlorite/illite) (Peretyazhko et al., 2012). Mössbauer spectral parameters for ferrihydrite, however, are slightly different than pure ferrihydrite (Chen et al., 2015), and this could be due to the coating of the oxide with P or organic matter (OM) (Joshi et al., 2015; Chen et al., 2015). It is noteworthy to mention that nanogoethite, a predominant Fe-oxide in some lake sediment (Zee et al., 2003), is absent in these sediments. Comparison of RT and 13 K spectra, coupled to XRD results, further suggests the Fe(II) doublet feature in the spectra is primarily due to Fe(II) in chlorite/illite rather than siderite (FeCO<sub>3</sub>) and vivianite [Fe<sub>2</sub>(PO<sub>4</sub>)<sub>3</sub>]. This is because siderite and vivianite display octet feature at 13 K (Peretyazhko et al., 2012; Murad and Cashion, 2004). It is also likely that a small fraction of the Fe(II) doublet could be due to Fe(II) in feldspars (Dyar et al., 2002).

The differences in Mössbauer spectral features between 1-cm and 20-cm sediments are striking. The ferrihydrite-like phase is absent in the 20-cm sediment (Fig. 6b-1 and b-2). The amount of ilmenite (FeTiO<sub>3</sub>), shown by black doublet (Fig. 6b-1 and b-2), is quite high in the 20-cm sediment compared to that in 1-cm sediment. The Fe(III)/Fe(II) ratio suggests that sediments are relatively more reduced in the 20-cm depth than in the 1-cm, similar to a previous publication

(Kukkadapu et al., 2006). It is possible the Fe(II) doublet feature could have contributions from sorbed Fe(II) (Fox et al., 2013).

# 3.5. Isotopic compositions of different P pools

Fig. 7 depicts the  $\delta^{18}O_P$  values in different P pools as a function of sediment depths (the data are listed in Table S1). Overall,  $\delta^{18}O_P$  values of each P pool are distinct and consistently similar across the depth of sediment studied. The order of  $\delta^{18}O_P$  values generally follows as Albound P > Fe-bound P > exchangeable P > authigenic P > detrital P, except a few outliers. On the basis of the measured  $\delta^{18}O_w$  values of pore water (-6.3 to -7.1%) and mean measured temperature of 18.2 °C at the sediment-water interface, the calculated equilibrium isotope value (according to Eq. (1)) is 16.0–16.7% (Fig. 7). However, the surface water temperature of the lake varies highly from 6 to 30 °C from winter to summer (Oin et al., 2002), but the temperature at the sedimentwater interface is limited within 16.5–25.8 °C from late Spring to early Fall (Zeng et al., 2018). This variation adds some uncertainty and deviation of equilibrium isotope values. Nonetheless, calculation using measured temperature and water isotopes shows most of the measured isotope data are out of equilibrium. For example, measured  $\delta^{18}O_P$  values for detrital P and authigenic P pools are lighter than equilibrium, while that of Fe- and Al-bound P are distinctly heavier. Al-bound P becomes slightly lighter with depth with the heaviest  $\delta^{18}O_P$  value of 23.35 ( $\pm$ 0.31)%. Additionally, exchangeable P is close to equilibrium and varies within a narrow range of 17.09 to 18.47‰. The isotopic compositions of detrital P are the lightest among all measured P pools with  $\delta^{18}O_P$ values between 9.76 and 14.62%. A unique difference is that the  $\delta^{18}O_P$ values of ferric Fe-bound P are significantly lighter than Al-bound P at the upper layer of the sediment profile. This difference, however, is largely erased at 7 cm and downwards.

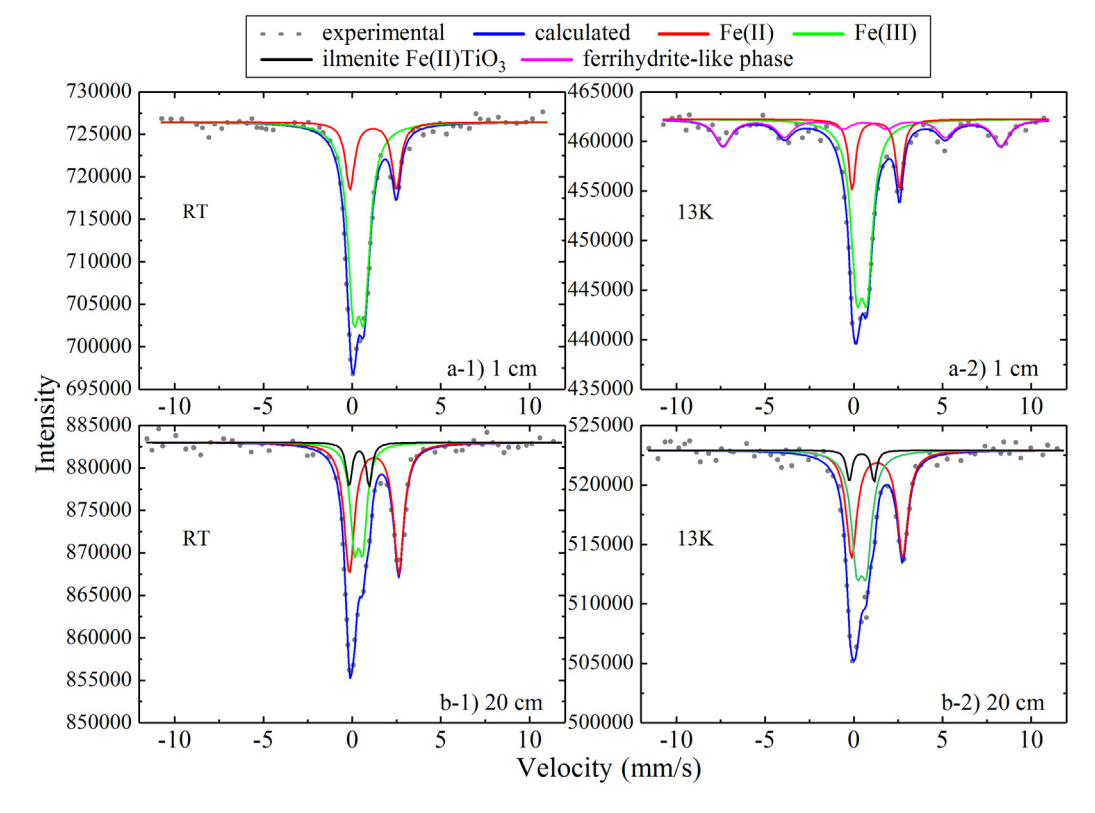


Fig. 6. Mössbauer spectra of selected (top and bottom at 1 and 20 cm depth, respectively) sediment layers at room temperature (a-1, b-1) and at 13 K (a-2, b-2). Dotted lines refer to measured experimental data, and colored line traces are model fittings which show relative contributions of various Fe-phases. Spectra were fitted with Lorentzian lineshapes using the least square method.

**Table 2**Mössbauer fitting parameters for top and bottom layers of sediment column. Modeling was carried out using Lorentzian line shape model (Recoil™ Software).

Measured sample depth	Measurement temperature	Mössbauer paramete	rs <sup>a</sup>	Iron compounds assignment/mineral		
		Magnetic splitting	δ (mm/s)	$\Delta E_Q$ (mm/s)	H <sub>hf</sub> Koe	
1 cm	RT	Doublet 1	0.373(19)	0.617(33)	=	Fe(III), mix of clay and ferrihydrite
		Doublet 2	1.184(38)	2.613(72)	_	Fe(II), chlorite/illite
		Doublet 1	0.457(17)	0.601(29)	_	Fe(III), clay
	13 K	Doublet 2	1.240(26)	2.676(49)	_	Fe(II), chlorite
		Sextet 1	0.540(77)	-	485.5(50)	Fe(III), ferrihydrite
20 cm	RT	Doublet 1	1.235(43)	2.783(83)	-	Fe(II), clay
		Doublet 2	0.363(34)	0.480(16)	_	Fe(III), clay
		Doublet 3	0.393(84)	1.130(21)	-	Fe(II), ilmenite
		Doublet 1	1.315(37)	2.875(72)	-	Fe(II), clay
	13 K	Doublet 2	0.439(36)	0.550(14)	-	Fe(III), clay
		Doublet 3	0.442(75)	1.390(18)	_	Fe(II), ilmenite

The values in parenthesis refer to the uncertainties of the measure data (in accordance with the last significant figure), for example, 0.373(19) means  $0.373 \pm 0.019$ .

#### 4. Discussion

# 4.1. Spectroscopy analyses

XRD patterns and Mössbauer spectra suggest that chlorite (a phyllosilicate mineral), ferrihydrite like Fe-oxyhydroxide, and pyrite are the dominant Fe minerals. Higher concentrations of insoluble Fe(II) fraction in the deeper sediment quantified using 13 K Mössbauer spectra suggests a stronger anoxic condition in the deeper sediment (Table 3). The decrease in the Fe(III)/Fe(II) ratio which becomes ~1 at 20 cm depth (Table 3) also suggests that the Fe in the sediment is highly reduced (Kukkadapu et al., 2006). Intriguingly, authigenic Fe(II) minerals such as vivianite were not detected by XRD and could not be confirmed by Mössbauer spectroscopy. The reason for the absence of vivianite is speculated to be due to the partial oxygenation of sediments during shoaling

(wind-driven disturbance) in shallow water (mean depth of 2.5 m) and not favoring its precipitation.

# 4.2. Characteristics of sediment P pools

Characteristic trends of different P pools provide information on their deposition or precipitation in the sediment column. For example, detrital P pools are relatively stable with concentration at 3.33 ( $\pm 0.53$ ) µmol/g. This implies a constant loading of detrital sediment of sedimentary, igneous, or metamorphic origin to the Zhushan Bay and the higher resistance to dissolution of this P pool under repeated anoxia reported previously (Jaisi and Blake, 2010). Authigenic P pool shows a generally increasing trend with depth, except a very few outliers, indicating continued precipitation of authigenic P minerals during early diagenesis. High concentrations of Ca and  $P_i$  in pore water (Fig. 1) are expected to facilitate the precipitation of a

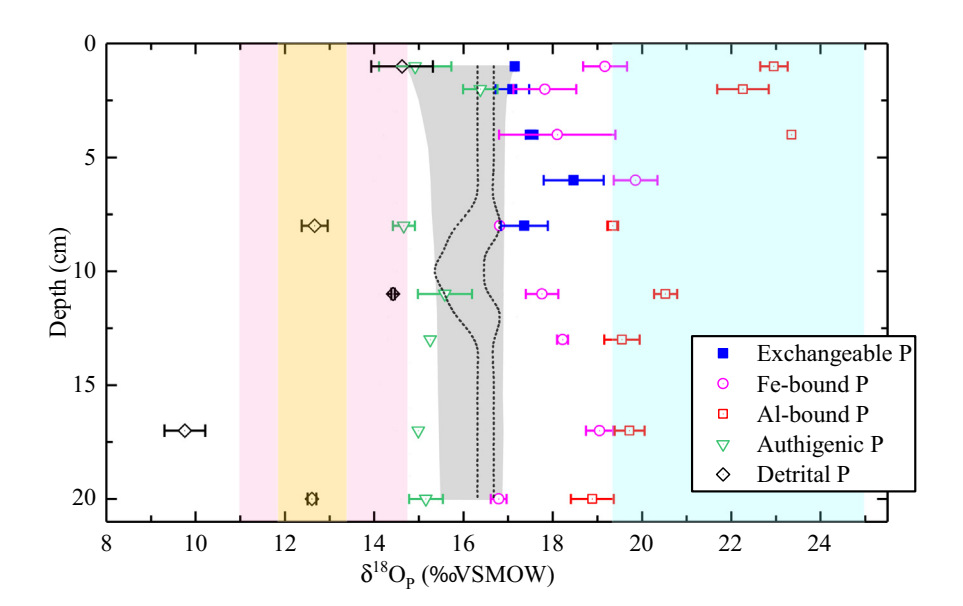


Fig. 7. The  $\delta^{18}$ O<sub>P</sub> values in different P pools and potential sources in the sediment. Gray shaded region represents the equilibrium  $\delta^{18}$ O<sub>P</sub> values zone calculated using season-average temperature data at sediment-water interface (Zeng et al., 2018). Area between dashed lines in grey zone denotes the range of equilibrium isotope values (with 95% confidence level) calculated using measured temperature at sediment-water interface and porewater isotope values in June. Light pink field refers to the  $\delta^{18}$ O<sub>P</sub> values of igneous/metamorphic origin (11–14.7%; see Jaisi and Blake (2010)); light yellow field represent freshly regenerated P<sub>i</sub> with  $\delta^{18}$ O<sub>P</sub> values between 11.90 and 13.33% from phosphoesters (calculated as in Joshi et al., 2015) and light cyan field represents the ranges of chemical fertilizers with reported  $\delta^{18}$ O<sub>P</sub> values in overall range of 19.4–25.0% (Gruau et al., 2003; McLaughlin et al., 2006; Li et al., 2011; Gross et al., 2013). The values with error bar were the means and standard deviations of three replicate analyses.

 $<sup>^{</sup>a}$   $\delta=$  isomer shift (mm/s);  $\Delta E_{Q}=$  quadrupole splitting (mm/s);  $H_{hf}=$  hyperfine magnetic field; RT= room temperature, respectively.

**Table 3**Measured Fe fraction and ratio for top and bottom layers of sediment column using <sup>57</sup>Fe-Mössbauer spectroscopy at 13 K. The fraction ratio was calculated from the ratio of individual peak corresponding to different Fe phases.

Measurement temperature	Valence state	Sediment layer		
		1 cm	20 cm	
13 K	Fe(III)	83.1%	52%	
	Fe(II)	16.9%	48%	
	Fe (III)/Fe(II)	4.9	1.1	

metastable precursor followed by crystalline apatite (Liang and Blake, 2007). Redox change caused by microbial activity may further accelerate the precipitation of apatite in the interface environment by providing localized chemical gradients and associated pH shifts in the sediment porewater (Krzysztof et al., 1994).

Besides terrigenous input of Al-containing minerals, dissolved Al in the water column could hydrate and form colloidal Al hydroxides with large specific surfaces and strong binding ability to P<sub>i</sub> (Reitzel et al., 2009) and precipitate as endogenetic Al-P minerals. Elevated fresh Al (oxy)hydroxide content in the upper sediment could scavenge P<sub>i</sub> released from ferric (oxy)hydroxides during anoxia and limit the upward flux, Significant formation of solid-phase Al(OH)<sub>3</sub> occurs within the pH range of 5.5–9.0 (Huser and Rydin, 2005). Under the alkalescent conditions (at pH 7–7.5) in the sediment of the Zhushan Bay, re-precipitation of Al-P minerals is expected (Reitzel et al., 2013). Once precipitated, Al (OH)<sub>3</sub> is stable under low redox conditions. Relatively low values and the random variation of Al in the pore water could be an indication of the formation of Al-bound P pool. The possibility of the formation of Al-bound P forms in the sediment, however, needs further corroborative evidence.

The Fe-bound P is the most predominant P pool in the sediment. A sharp decrease in Eh with depth suggests that sediment below 2 cm remains largely anoxic (Fig. 2), but the anoxic depth may become shallower during phytoplankton blooms followed by hypoxic bottom water in late spring. The increase in Fe(II) concentration with the sediment depth (Table 3) also supports the shallow oxic-anoxic boundary and dissolution of Fe (oxy)hydroxides (Yu et al., 2017). During hypoxia, Fe(III) is reduced to Fe(II), which has higher solubility, and P<sub>i</sub> bound to Fe(III) minerals is released into the pore water. This allows the diffusion of P<sub>i</sub> upwards into overlying water as an endogenous P<sub>i</sub> input source.

Even though Fe(oxy)hydroxides may not be completely dissolved during episodes of anoxia in the sediment (Joshi et al., 2015), the amount of  $P_i$  derived from ferric Fe-bound P is expected to be high due to the size of this P pool.

#### 4.3. Potential sources of detrital P

The obvious presence of non-expandable clay minerals (e.g., chlorite, illite, and kaolinite) suggests terrigenous sources of sediment as well as significant diagenesis in the sediment column. P initially originating from magmatic and/or metamorphic sources is conservatively solubilized via weathering and dissolution/re-precipitation actions during pedogenesis and  $\delta^{18}O_P$  values could be preserved or equilibrate with ambient percolating and meteoric water (Fox et al., 2013). The narrow ranges of  $\delta^{18}O_P$  values (9.76–14.62%) of detrital P in the sediment profile, which are lighter than equilibrium values (16.0-16.7%) and close to that in Peru Margin sediment (12.6–15.4%) suggest the potential sources from igneous or metamorphic origin (5.0-14.7%; Jaisi and Blake, 2011; Mizota et al., 1992; Taylor, 1968). An outlier (lighter) isotope value at ~17 cm (9.76  $\pm$ 0.46%) approaching magmatic  $\delta^{18}O_P$  values (<8%, see Blake et al., 2010) suggests potential mixing of these two end-member sources in variable proportions. However,  $\delta^{18}O_P$  values of detrital P in Zhuanshan Bay distinctly deviated from  $\delta^{18}O_P$  values of authigenic P and site-specific equilibrium P. The conspicuous off-equilibrium isotope values indicate the resistance of detrital P against biogeochemical alteration in the sediment and preservation of the primary isotope signature during erosion, transport, and sedimentary processes. These findings further prove that the detrital P derived from the terrestrial origin is the most recalcitrant P pool and not bioavailable in the sediment column.

# 4.4. Potential sources of authigenic P

The isotopic compositions of authigenic P were less variable (15.28  $\pm$  0.56‰) among all P pools and remained relatively unchanged throughout the entire sediment column. This range is generally within the range of equilibrium  $\delta^{18} O_P$  values calculated using average season temperature at the sediment-water interface of Taihu Lake and close to the values measured in a similarly eutrophic Chesapeake Bay (Joshi et al., 2015). While the dissolved  $P_{i\nu}$  irrespective of sources, could precipitate into authigenic P, enzyme-catalyzed

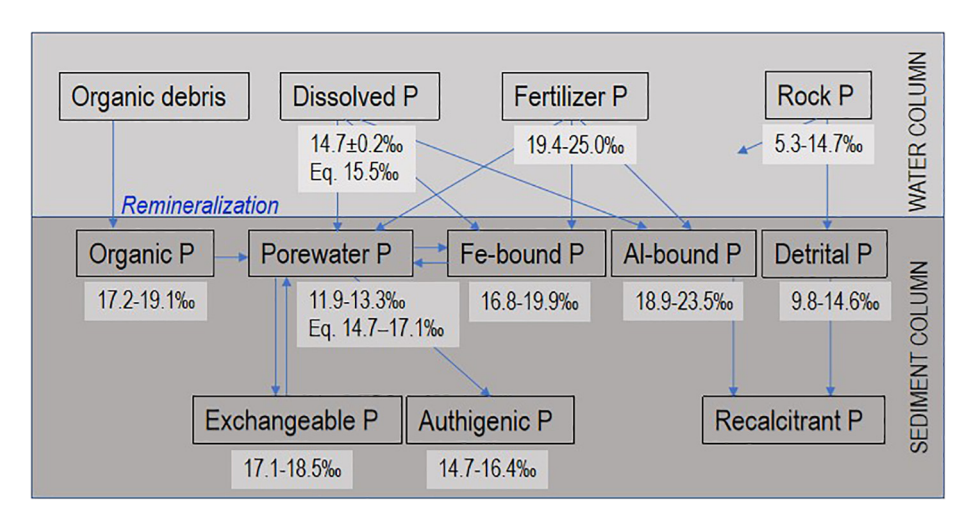


**Fig. 8.** Schematic representation of different pathways of P cycling and reactions that control phosphate oxygen isotopic compositions of different P pools at the sediment-water interface. The isotopic values of organic P are taken from Joshi et al. (2015), and that of igneous/metamorphic sources are from refs Jaisi and Blake (2010), Mizota et al. (1992) and Taylor (1968). Term 'Eq.' denotes equilibrium isotopic compositions.

hydrolysis of organic debris and subsequent release of P<sub>i</sub> has been found to be a major source of P precipitated into authigenic P minerals (Ruttenberg and Berner, 1993). Relatively lighter  $\delta^{18}O_P$  values of authigenic P possibly mean that any loosely sorbed P with heavier  $\delta^{18}O_P$  values than equilibrium did not contribute to this pool (see below). The hydrolytic mineralization and regeneration of P<sub>i</sub> from phosphoesters and polyphosphate result in the incorporation of nucleophilic oxygen from ambient water into Pi and subsequently change toward equilibrium (Colman et al., 2005). Remineralization of organic P to P<sub>i</sub> via intracellular and extracellular enzymes can induce an isotope fractionation of -10% to -30% depending on the enzymes involved (Liang and Blake, 2006, 2009) and this results in the overall lighter than equilibrium isotopic values calculated using measured water temperature in June. A preliminary isotope mass balance calculation suggested that the  $\delta^{18}O_P$  values of freshly regenerated P<sub>i</sub> from phosphoesters could lie at 11.90-13.33% (calculated using the method used in Joshi et al., 2015). This range is slightly lighter than the  $\delta^{18}O_P$  values of authigenic P in the Zhushan Bay, which could be due to a subsequent partial biological activity of the fresh P<sub>i</sub> – which results in the excursion of  $\delta^{18}O_P$  values toward equilibrium (Blake et al., 2001; Colman et al., 2005). The oxygen isotope exchange is very rapid during biological reactions and completes generally within few days to weeks (Stout et al., 2014). However, controlled laboratory experiments have revealed negligible isotope fractionation between dissolved P<sub>i</sub> and apatite (Liang and Blake, 2007). This result suggests that fast nucleation of numerous metastable phosphate intermediates or a precursor phase of apatite due to supersaturation of P in the pore solution and subsequent formation of apatite minerals (Krzysztof et al., 1994) may not impart any isotope variation. Once precipitated, the isotopic composition of authigenic P is faithfully locked in and may remain largely unaltered (Liang and Blake, 2007; Blake et al., 2010; Jaisi and Blake, 2010).

# 4.5. Potential sources of Al-bound P

To our knowledge, this is the first report of  $\delta^{18}O_P$  values of Al-bound P in the sediment, which lies within a narrow range (18.9–23.35%). Since this range is out of equilibrium, it further implies the possibility of identifying certain sources. Laboratory experiments illuminated that the formation of reactive polynuclear hydroxo complexes by the hydrolyzing cations from pore water induces the subsequent oxolation process and phosphate adsorption (Lijklema, 1980). The Al oxyhydroxide is stable and has strong sorption capacity under either oxic or anoxic conditions once pH is circumneutral in natural environments (Lijklema, 1980), and prevents release of P from the sediment phase during anoxia. This means that  $\delta^{18}O_P$  values of Al bound P should better preserve the isotope signature of source P<sub>i</sub>. Significantly more positive excursion than equilibrium isotopes of the Al-bound P pool indicates that the sediment could have originated from the conversion of other P phases that have heavier  $\delta^{18}O_P$  values. However, further confirmation on the potential sources and processes that can generate heavy isotopic compositions is needed.

Various chemical P fertilizers are applied in the upland agricultural soils of the catchment for agricultural and recreational purposes and may be lost from soil, reaching aquatic environments (Ruttenberg, 1992; Young et al., 2009). Chemical fertilizers are manufactured from mined phosphorite deposits, and oxygen isotope composition of phosphorite is controlled by the environment in the sedimentary basin and is expected to be unaltered during manufacturing and preparing processes (Gruau et al., 2005), which are all chemical reactions. The  $\delta^{18}{\rm O}_{\rm P}$  values of chemical fertilizers reported in the literature are in the overall range of 19.6–23.1% (Gruau et al., 2005), 19.4–20.5% (McLaughlin et al., 2006), 20.9–25.0% (Li et al., 2011) and 21.8–22.8% (Gross et al., 2013). Fertilizer sources of P in the soil can be captured by colloidal Al-(oxy)hydroxides and then transported to the lake water. Exogenetic

Al mineral bound P is expected to be conservatively transported to the water and settle to sediment for subsequent burial. Since Al-(oxy)hydroxides are insoluble and immobile in alkalescent environments, both biotic and abiotic processes are expected not to exert significant influence on the transformation of Al-bound P in the sediments and the isotope signatures are expected to be preserved. Please note that allochthonous sources of Al-bound P was not independently confirmed in this study and the verification of isotope fidelity of this pool during transport and deposition is needed. However, the ranges of isotope values heavier than Fe-bound P and fertilizer sources provide some indication of their terrestrial origin. In this case, Al-bound P in the sediment could serve as a more resistant sink of P that ferric Fe-bound P (see below).

# 4.6. Potential sources of ferric Fe-bound P

The isotopic values of ferric Fe-bound P vary from 16.79 to 19.86% and lie between equilibrium and Al-bound P isotope values, Joshi et al. (2015) proposed that the  $\delta^{18}O_P$  values (18.7–20.8%) of some ferric Fe-bound P in the sediment in the Chesapeake Bay might have remained unchanged and retained their heavier than equilibrium isotope values. Similar to Al-bound P, the dominant proportion of ferric Fe-bound P may also potentially derive from terrestrial sources including chemical fertilizers. The difference, however, is the stability of ferric Fe minerals which undergo reductive dissolution under hypoxic/anoxic conditions in the sediment profile as indicated by lower Eh values in deeper sediment (Fig. 2j) and low penetration depth of oxygen (Zhang et al., 2014). Dissolved Fe<sup>2+</sup> can diffuse and could precipitate under oxidizing/aerobic conditions due to change in season, winddriven shoaling, or bioturbation. Isotope labeling experiments have proved the absence of O atom exchange between phosphate and oxygen in Fe and Mn-containing minerals during sorption and desorption reactions (Li and Jaisi, 2015). The dissolved P<sub>i</sub> released from the ferric Fe pool and other sources could undergo enzyme-mediated oxygen exchange with ambient water during biological cycling which alters the δ<sup>18</sup>O<sub>P</sub> values toward equilibrium. Recycled P<sub>i</sub> can subsequently be trapped by colloidal ferric (oxy)hydroxides once precipitated during aerobic periods and coprecipitated/occluded phosphate could preserve the  $\delta^{18}O_P$  values (Jaisi et al., 2011). This reaction makes  $\delta^{18}O_P$  values of the ferric Fe pool lighter than that of Al bound P, assuming that both P pools had heavier (Al-P like) than equilibrium isotopes to start with (Fig. 7). Integrating isotopic compositions of various pools and supplementing with other published data containing conceptual similarities to Joshi et al. (2015), an improved schematic outline of P cycling between water and sediment is developed for shallow freshwater and eutrophic Zhushan Bay in the Taihu Lake (Fig. 8). It shows that the overprint of isotope values from exogenous input such as fertilizer coupling with the endogenous release of ferric Fe-bound P via reductive dissolution appears to be the predominant reactions that contribute to high dissolved P<sub>i</sub> in this study site. This source of P could diffuse to the surface and near-surface water to fuel mid- and late-stage eutrophication in Taihu Lake.

# 5. Conclusions

Our research differentiates the  $\delta^{18}O_P$  values and source groups of different P pools in the sediment from a shallow freshwater lake. Authigenic P with  $\delta^{18}O_P$  values below equilibrium principally originates from the degradation and re-mineralization of organic debris due to phosphoenzyme hydrolysis and remains as occluded/recalcitrant P pool together with detrital P from terrigenous sources. It appears that  $\delta^{18}O_P$  values of Al-bound P are relatively good indicator of the terrigenous provenance because this P pool is generally unaltered than Febound P. The  $P_i$  derived from exogenous input such as fertilizers coupling with endogenous release from remineralization and reductive dissolution of Fe-bound P together contribute to the high concentration in

the water column and could fuel eutrophication in the shallow freshwater lake system like Taihu.

#### Acknowledgments

This research was funded by National Science Foundation (1738770 and 1757353), National Natural Science Foundation of China (41503099), Natural Science Foundation of Jiangsu Province (BK20150902, BK20170948) and China Scholarship Council (CSC). We would like to thank Oi Lin, Zhenzhen Yu, and Huiji Liu for the sample preparation, Xiaoke Zhang for XRD analyses, and Tosun Gulcin for the help on isotope measurement. A portion of the work is carried out at Environmental Molecular Sciences Laboratory, Pacific Northwest National Laboratory, Richland, WA 99354, USA.

# Appendix A. Supplementary data

Supplementary data to this article can be found online at https://doi. org/10.1016/j.scitotenv.2019.04.322.

#### References

- Blake, R.E., Jeffrey, C., Alt, J.C., Anna, M., Martini, A.M., 2001. Oxygen isotope ratios of PO<sub>4</sub>: an inorganic indicator of enzymatic activity and P metabolism and a new biomarker in the search for life. PNAS 98, 2148-2153.
- Blake, R.E., O'Neil, J.R., Surkov, A.V., 2005. Biogeochemical cycling of phosphorus: insights from oxygen isotope effects of phosphoenzymes. Am. J. Sci. 305, 596-620.
- Blake, R.E., Chang, S.J., Lepland, A., 2010. Phosphate oxygen isotopic evidence for a temperate and biologically active Archaean ocean. Nature 464, 1029-1032.
- Chang, S.J., Blake, R.E., 2015. Precise calibration of equilibrium oxygen isotope fractionations between dissolved phosphate and water from 3 to 37 °C. Geochim. Cosmochim. Acta 150, 314-329.
- Chen, C., Kukkadapu, R.K., Sparks, D.L., 2015. Influence of coprecipitated organic matter on  $Fe_{(aq)}^{2+}$ -catalyzed transformation of ferrihydrite and carbon mobility. Environ. Sci. Technol. 49, 10927-10936.
- Cohn, M., Urey, H.C., 1938. Oxygen isotope exchange reactions of organic compounds and water. J. Am. Chem. Soc. 60, 679-682.
- Colman, A.S., Blake, R.E., Karl, D.M., Fogel, M.L., Turekian, K.K., 2005. Marine phosphate oxygen isotopes and organic matter remineralization in the oceans. PNAS 102,
- Davies, C.L., Surridge, B.W.J., Gooddy, D.C., 2014. Phosphate oxygen isotopes within aquatic ecosystems: global data synthesis and future research priorities. Sci. Total Environ, 496, 563-575
- Deng, J.M., Paerl, H.W., Qin, B.Q., Zhang, Y.L., Zhu, G.W., Jeppesen, E., Cai, Y.J., Xu, H., 2018. Climatically-modulated decline in wind speed may strongly affect eutrophication in shallow lakes. Sci. Total Environ. 645, 1361-1370.
- Dyar, M.D., Housely, R.M., Stiltner, S.A., 2002. Mössbauer study of <sup>57</sup>Fe-doped synthetic anorthite: implications for interpretation of lunar anorthite spectra. Lunar Planet. Sci. XXXIII, 1725 (Houston, Texas, USA).
- Elsbury, K.E., Paytan, A., Ostrom, N.E., Kendall, C., Megan, B., Young, M.B., McLaughlin, K., Rollog, M.E., Watson, S., 2009. Using oxygen isotopes of phosphate to trace phosphorus sources and cycling in Lake Erie. Environ. Sci. Technol. 43, 3108-3114.
- Fink, G., Alcamo, J., Flörke, M., Reder, K., 2018. Phosphorus loadings to the world's largest lakes: sources and trends. Glob. Biogeochem. Cycles 32, 617-634.
- Fox, P.M., Davis, J.A., Kukkadapu, R.K., Singer, D.M., Bargar, J., Williams, K.H., 2013. Abiotic U(VI) reduction by sorbed Fe(II) on natural sediments. Geochim. Cosmochim. Acta 117, 266-282
- Gächter, R., Wehrli, W., 1998. Ten years of artificial mixing and oxygenation: no effect on the internal phosphorus loading of two eutrophic lakes, Environ, Sci. Technol, 32, 3659-3665.
- Gross, A., Nishri, A., Angert, A., 2013. Use of phosphate oxygen isotopes for identifying atmospheric-P sources: a case study at Lake Kinneret. Environ. Sci. Technol. 47, 2721-2727.
- Gruau, G., Legeas, M., Riou, C., Gallacier, E., Martineau, F., Hénin, O., 2005, The oxygen isotope composition of dissolved anthropogenic phosphates: a new tool for eutrophication research? Water Res. 39, 232-238.
- Huser, B.I., Rydin, E., 2005. Phosphorus inactivation by aluminum in Lakes Gårdsjön and Härsvatten sediment during the industrial acidification period in Sweden, Can. I. Fish. Aguat. Sci. 62, 1702-1709.
- Jaisi, D.P., Blake, R.E., 2010. Tracing sources and cycling of phosphorus in Peru Margin sediments using oxygen isotopes in authigenic and detrital phosphates. Geochim. Cosmochim, Acta 74, 3199-3212.
- Jaisi, D.P., Blake, R.E., 2014. Advances in using oxygen isotope ratios of phosphate to understand phosphorus cycling in the environment. Adv. Agron. 125, 1–54.
- Jaisi, D.P., Kukkadapu, R.K., Stout, L.M., Varga, T., Blake, R.E., 2011. Biotic and abiotic pathways of phosphorus cycling in minerals and sediments: insights from oxygen isotope ratios in phosphate. Environ. Sci. Technol. 45, 6254-6261.

- Joshi, S.R., Kukkadapu, R.K., Burdige, D.J., Bowden, M.E., Sparks, D.L., Jaisi, D.P., 2015. Organic matter remineralization predominates phosphorus cycling in the mid-bay sediments in the Chesapeake Bay. Environ. Sci. Technol. 49, 5887-5896.
- Joshi, S.R., Li, W., Bowden, M., Jaisi, D.P., 2018. Sources and pathways of formation of recalcitrant and residual phosphorus in an agricultural soil. Soil Syst. 2, 45.
- Karl, D.M., 2000. Phosphorus, the staff of lie. Nature 406, 31–33. Krzysztof, P., Krajewski, K.P., Van Cappellen, P., Trichet, J., Kuhn, O., Lucas, J., Martin-Algarra, A., Prévôt, L., Tewari, V.C., Gaspar, L., Knight, R.I., Lamboy, M., 1994. Biological processes and apatite formation in sedimentary environments. Eclogae Geol. Helv. 87. 701–745.
- Kukkadapu, R.K., Zachara, J.M., Fredrickson, J.K., McKinley, J.P., Kennedy, D.W., Smith, S.C., Dong, H.L., 2006. Reductive biotransformation of Fe in shale-limestone saprolite containing Fe(III) oxides and Fe(II)/Fe(III) phyllosilicates. Geochim. Cosmochim. Acta 70, 3662-3676
- Lecuyer, C., Grandjean, P., Sheppard, S.M.F., 1999. Oxygen isotope exchange between dissolved phosphate and water at temperatures ≤135 °C: inorganic versus biological fractionations, Geochim, Cosmochim, Acta 63, 855-862.
- Li, H., Jaisi, D.P., 2015. An isotope labeling technique to investigate atom exchange during phosphate sorption and desorption. Soil Sci. Soc. Am. J. 79, 1340-1351.
- Li, X., Wang, Y., Stern, J., Gu, B.H., 2011. Isotopic evidence for the source and fate of phosphorus in Everglades wetland ecosystems, Appl. Geochem. 26, 688-695.
- Liang, Y., Blake, R.E., 2006. Oxygen isotope signature of Pi regeneration from organic compounds by phosphomonoesterases and photooxidation. Geochim. Cosmochim. Acta 70, 3957-3969.
- Liang, Y., Blake, R.E., 2007. Oxygen isotope fractionation between apatite and aqueousphase phosphate: 20-45 °C. Chem. Geol. 238, 121-133.
- Liang, Y., Blake, R.E., 2009. Compound- and enzyme-specific phosphodiester hydrolysis mechanisms revealed by  $\delta^{18}$ O of dissolved inorganic phosphate: implications for marine P cycling. Geochim. Cosmochim. Acta 73, 3782-3794.
- Lijklema, L., 1980. Interaction of orthophosphate with iron(III) and aluminum hydroxides. Environ. Sci. Technol. 14, 537-541.
- Linge, K.L., Carolyn, E., Oldham, C.E., 2004. Control mechanisms for dissolved phosphorus and arsenic in a shallow lake. Appl. Geochem. 19, 1377-1389.
- Longinelli, A., Nuti, S., 1973. Revised phosphate-water isotopic temperature scale. Earth Planet. Sci. Lett. 19, 373-376.
- Markel, D., Kolodny, Y., Luz, B., Nishri, A., 1994. Phosphorus cycling and phosphorus sources in Lake Kinneret: tracing by oxygen isotopes in phosphate. Isr. J. Earth Sci. 43, 165-178
- McLaughlin, K., Kendall, C., Silva, S.R., Young, M., Paytan, A., 2006. Phosphate oxygen isotope ratios as a tracer for sources and cycling of phosphate in North San Francisco Bay, California. J. Geophys. Res. 111, G03003.
- Mizota, C., Domon, Y., Yoshida, N., 1992. Oxygen isotope composition of natural phosphates from volcanic ash soils of the great rift-valley of Africa and East Java, Indonesia. Geoderma 53, 111-123.
- Murad, E., Cashion, J., 2004. Mossbauer Spectroscopy of Environmental Materials and Their Industrial Utilization. Kluwer Academic Publishers, Norwell, Massachusetts,
- Peretyazhko, T.S., Zachara, J.M., Kukkadapu, R.K., Heald, S.M., Kutnyakov, I.V., Resch, T.M., Arey, B.W., Wang, C.M., Kovarik, L., Phillips, J.L., Moore, D.A., 2012. Pertechnetate (TcO<sub>4</sub>) reduction by reactive ferrous iron forms in naturally anoxic, redox transition zone sediments from the Hanford Site, USA. Geochim. Cosmochim. Acta 92, 48-66.
- Pucéat, E., Joachimski, M.M., Bouilloux, A., Monna, F., Bonin, A., Motreuil, S., Morinière, P., Hénard, S., Mourin, J., Dera, G., Quesne, D., 2010. Revised phosphate-water fractionation equation reassessing paleotemperatures derived from biogenic apatite. Earth Planet Sci. Lett. 298, 135-142.
- Qin, B.Q., Hu, W.P., Chen, W.M., et al., 2002. Process and Mechanism of Environmental Changes of the Taihu Lake. Chinese Science Press, Beijing, pp. 97-98 (in
- Reed, D.C., Slomp, C.P., Gustafsson, B.G., 2011. Sedimentary phosphorus dynamics and the evolution of bottom-water hypoxia: a coupled benthic-pelagic model of a coastal system. Limnol. Oceanogr. 56, 1075-1092.
- Reitzel, K., Jensen, H.S., Flindt, M., Andersen, F.Ø., 2009. Identification of dissolved nonreactive phosphorus in freshwater by precipitation with aluminum and subsequent <sup>31</sup>P NMR analysis. Environ. Sci. Technol. 43, 5391-5397.
- Reitzel, K., Jensen, H.S., Egemose, S., 2013. pH-dependent dissolution of sediment aluminum in six Danish lakes treated with aluminum. Water Res. 47, 1409-1420.
- Ruttenberg, K.C., 1992. Development of a sequential extraction method for different forms of phosphorus in marine sediments. Limnol. Oceanogr. 37, 1460-1482.
- Ruttenberg, K.C., Berner, R.A., 1993. Authigenic apatite formation and burial in sediments from non-upwelling, continental margin environments. Geochim. Cosmochim. Acta 57, 991-1007.
- von Sperber, C., Kries, H., Tamburini, F., Bernasconi, S.M., Frossard, E., 2014. The effect of phosphomonoesterases on the oxygen isotope composition of phosphate. Geochim. Cosmochim. Acta 125, 519-527.
- Stout, L.M., Joshi, S.R., Kana, T.M., Jaisi, D.P., 2014. Microbial activities and phosphorus cycling: an application of oxygen isotope ratios in phosphate. Geochim. Cosmochim. Acta 138, 101-116.
- Taylor, H.P., 1968. The oxygen isotope geochemistry of igneous rocks. Contrib. Mineral. Petrol. 19, 1-71.
- Young, M.B., McLaughlin, K., Kendall, C., Stringfellow, W., Rollog, M., Elsbury, K., Donald, E., Paytan, A., 2009. Characterizing the oxygen isotopic composition of phosphate sources to aquatic ecosystems. Environ. Sci. Technol. 43, 5190-5196.
- Yu, J.H., Ding, S.M., Zhong, J.C., Fan, C.X., Chen, Q.W., Yin, H.B., Zhang, L., Zhang, Y.L., 2017. Evaluation of simulated dredging to control internal phosphorus release from sediments: focused on phosphorus transfer and resupply across the sediment-water interface. Sci. Total Environ. 592, 662-673.

- Yuan, H.Z., An, S.Q., Shen, J., Liu, E.F., 2014. The characteristic and environmental pollution records of phosphorus species in different trophic regions of Taihu Lake, China. Environ. Earth Sci. 71, 783–792.
- Zee, C.V.D., Roberts, D.R., Rancourt, D.G., Slomp, C.G., 2003. Nanogoethite is the dominant reactive oxyhydroxide phase in lake and marine sediments. Geology 31, 993–996.
- Zeng, Y., Zhu, J., Wang, Y.P., Hu, W.P., 2018. Changes of water temperature and heat flux at water-sediment interface, East Lake Taihu. J. Lake Sci. 30, 1599–1609 (in Chinese). Zhang, L., Liao, Q.J.Y., Gua, X.Z., He, W., Zhan, Z., Fan, C.X., 2014. Oxygen and phosphorus dynamics in freshwater sediment after the deposition of flocculated cyanobacteria and the role of tubificid Worms. J. Hazard. Mater. 266, 1–9.